



## Channeling characterization of defects in silicon: an atomistic approach

M. Bianconi <sup>a,\*</sup>, E. Albertazzi <sup>a</sup>, S. Balboni <sup>b</sup>, L. Colombo <sup>c</sup>, G. Lulli <sup>a</sup>, A. Satta <sup>a</sup>

<sup>a</sup> CNR-IMM-Sezione di Bologna, Via P. Gobetti 101, I-40129 Bologna, Italy

<sup>b</sup> CeSIA-Settore Reti e Comunicazioni, Università di Bologna, Viale Filopanti 3, I-40126 Bologna, Italy

<sup>c</sup> INFN-SLACS and Dipartimento di Fisica, Università degli Studi di Cagliari, Cittadella Universitaria, I-09042 Monserrato (Cagliari), Italy

Available online 21 January 2005

---

### Abstract

We review here the possibilities opened by a recent development of the Monte Carlo binary collision approximation (MC-BCA) simulation of Rutherford backscattering spectrometry-channeling (RBS-C) spectra for the study of radiation damage in monocrystalline materials. The ion implantation of silicon has been chosen as a case study. Atomic-scale modeling of defect structures was used to determine the location of interstitial atoms in the host lattice. Among possible candidate defects, we have considered the elementary hexagonal, tetrahedral,  $\langle 110 \rangle$ -split interstitials, the Bond-defect and one type of tetra-interstitial cluster. For each defect model a large Si supercell was populated with a proper defect depth distribution and then it was structurally relaxed by the application of the classical EDIP potential. This model system was then given as an input to the MC-BCA simulation code and the spectra corresponding to nine different axial and planar alignments were calculated. For low defect concentration (a few atomic percent), the scattering yields are strongly dependent on the orientation and a distinct signature characteristic of the limited number of allowed interstitial positions in Si could be found. The comparison of simulations and experiments in the case of 180 keV self ion implantation allowed the identification of the dominant interstitial defect whose structural properties are represented by the split- $\langle 110 \rangle$  interstitial. By increasing the concentration of defects (and their mutual interaction) the technique loses sensitivity and, at the same time, the contribution of lattice relaxation becomes important. Under these conditions, although the RBS-C response becomes similar to the one obtained from a random distribution of displaced atoms, the major structural features of a heavily damaged sample could be still observed.

© 2004 Elsevier B.V. All rights reserved.

PACS: 61.85; 61.72.D

Keywords: RBS-channeling; Defects; Silicon; Ion implantation

---

\* Corresponding author. Tel.: +39 051 639 9140; fax: +39 051 639 9216.

E-mail address: [bianconi@lamel.bo.cnr.it](mailto:bianconi@lamel.bo.cnr.it) (M. Bianconi).

## 1. Introduction

One of the most peculiar features of the ion channeling techniques is the high sensitivity to the position of atoms displaced from regular lattice sites [1]. These techniques are mainly used to analyze a large class of small defects that are not resolved by transmission electron microscopy. As an example, when the signal of an impurity can be separated from that of the matrix element(s), triangulation procedures based on multi-axial experiments are commonly used for foreign atoms location [2]. The interpretation of data requires the support of Monte Carlo binary collision approximation (MC-BCA) calculations [3–5]. Standard simulation programs, in spite of the high degree of sophistication in the description of the beam penetration into the crystal, suffer a simplified description of defects. A deeper physical insight on the actual location, structure and binding properties of defects to the host lattice is indeed necessary to improve our current understanding of ion channeling experiments. Investigations in this field can take advantage of the recent great deal of atomic-scale modeling of the structure of small defects [6,7]. In the case of silicon, these studies have given relevant contribution to the understanding of the phenomena correlated to radiation damage [8] and, at the same time, they have produced a proliferation of computed defective structures in the literature. Although somewhere it has been discussed qualitatively the correlation between defect models and actual experiments [9,10], a quantitative treatment of such a link is still missing. The present work fits the above research scenario and is specifically addressed to this feature. We review the possibilities opened by a recent development of the standard MC-BCA code, allowing for the insertion of realistic defective structures within the simulation procedure of Rutherford backscattering spectrometry channeling (RBS-C) spectra. The core of this calculation is a large supercell, representative of a real sample, that it is populated with a proper depth distribution of a previously calculated defective structure and then it is structurally relaxed by the application of classical potentials [11]. As an example of this

method, some experiments concerning the defect recognition in Si implanted samples will be reported.

## 2. Experimental and computer simulation

Two (100) float zone *n*-type 500  $\Omega$  cm Si wafer were implanted at room temperature with 180 keV  $\text{Si}^+$  ions at a fluence of  $10^{14} \text{ cm}^{-2}$  (sample A) and  $10^{15} \text{ cm}^{-2}$  (sample B). These conditions produce a disorder distribution fully contained within a depth of 700 nm and with the maximum defect concentration located at about 200 nm. RBS-C measurements were performed using a 2 MeV  $\text{He}^+$  beam, and a backscattering angle of  $170^\circ$  under the seven axial  $\langle 111 \rangle$ ,  $\langle 112 \rangle$ ,  $\langle 113 \rangle$ ,  $\langle 100 \rangle$ ,  $\langle 130 \rangle$ ,  $\langle 120 \rangle$ ,  $\langle 110 \rangle$  and the two planar  $\{110\}$  and  $\{100\}$  alignments. Details of the measurement setup, which includes a Faraday chamber for absolute measurements (uncertainty in the yield  $\cong 2\%$ ), are reported in [12]. Virgin and thick ion-amorphized Si reference spectra were always measured together with the spectra of implanted samples.

The model sample for the simulation of RBS-C spectra was prepared as follows. A Si supercell containing about 2.2 million atoms was populated using only one kind of defect at a time, according to a depth distribution profile given in input. To balance excess interstitials and keep the number of atoms constant, a depth profile of single vacancies, equal to the one of interstitial atoms, was inserted. The exact defect locations at a certain depth were chosen at random, taking into account all the possible orientations of defects in the Si lattice and under the constraint that cluster–vacancy, cluster–cluster and vacancy–vacancy distances were the largest compatible with the local concentration of defects. An energy minimization procedure at constant volume and using periodic boundary conditions was applied to the supercell (more details on the procedure can be found in [11]). In this work we have used the environment-dependent interatomic potential (EDIP) [13] classical potential, which is known to give a good description of local bonding in bulk defects and disordered phases of Si.

Five different defect models have been considered: the elementary hexagonal ( $I_H$ ), tetrahedral ( $I_T$ ),  $\langle 110 \rangle$ -split ( $I_S$ ) interstitial, the Bond-defect (BD) and the  $I_{4b}$  cluster, which is formed by the agglomeration of four split- $\langle 100 \rangle$  interstitials on the  $\{100\}$  plane [14]. The initial coordinates of the defective atoms were taken from the results of tight-binding molecular dynamics calculations performed in 512-atom Si cells [15]. The BD defect [16] is considered to play an important role in the amorphization process of silicon [17,18]. We do not consider here the clusters  $I_k$  ( $k = 2, 3, 4$ ) obtained by the addition of  $(k - 1)$  interstitials to  $I_S$ , as we have already shown [19] that they give more or less closely the same RBS-C response of the simple  $I_S$ . In addition to the above mentioned models, simulations were also performed in the framework of the random model where defects consist of atoms randomly displaced from the original sites with no deformation induced in the surrounding lattice.

RBS-C spectra of the relaxed supercells with defects were simulated with the computer code BASIC [5] in which full calculation of He trajectories is performed according to the MC-BCA method. Using the concept of close encounter probability and approximating the path of a backscattered ion with a straight trajectory in a random medium, the program calculates the yield at the detector as a function of backscattering energy.

### 3. Basics of defects recognition by RBS-C

In order to understand the RBS-C response to the different kind of defects and to plan the most appropriate experimental procedures we make use of basic channeling concepts. In Fig. 1 we show the  $\langle 100 \rangle$  and  $\langle 110 \rangle$  projected distribution  $P(r)$  of the lattice atoms as a function of the distance  $r$  from the regular lattice sites computed for a supercell, obtained by  $10 \times 10 \times 10$  replicas of the unit diamond cell, with one  $I_S$  interstitial placed in the centre and structurally relaxed by the EDIP potential. The distributions are averaged over the equivalent orientations of the defect. All the atoms displaced within  $r \leq \rho$  ( $\rho \cong 0.11 \text{ \AA}$  is the 2D r.m.s. vibrational amplitude) do not inter-

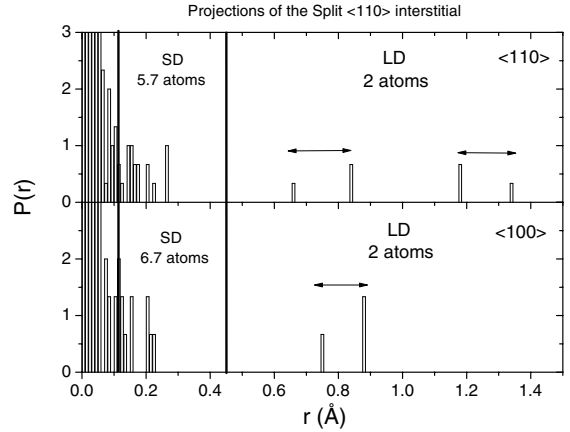


Fig. 1.  $\langle 100 \rangle$  and  $\langle 110 \rangle$  projected distribution  $P(r)$  of the lattice atoms as a function of the distance  $r$  from the regular lattice sites computed for a  $20 \times 20 \times 20$  atoms Si supercell with one  $I_S$  interstitial placed in the centre (see text and Table 1).

act with the channelled beam. For both alignments a group of  $\sim 6$  slightly displaced (SD) atoms is distributed in the range  $\rho < r < R_L$  where  $R_L = 0.45 \text{ \AA}$  is the radius of the Lindemann sphere [11]. The last group ( $r > R_L$ ) consists of the projections of the two largely displaced (LD) atoms of the  $I_S$  dumbbell. It is worth noting that the SD atoms are distributed within a volume of about  $500 \text{ \AA}^3$  around the interstitial. Interaction between  $I_S$  interstitials is then expected for concentrations of the order of 4%. A similar classification of the  $P(r)$  was already proposed by Weber et al. [9]. Their results are only in qualitative agreement with those of Fig. 1 as they used a different atomic potential. The characteristic parameters of the projected distributions, for the defect models here considered, are summarized in Table 1. As long as one isolated interstitial is considered, each defect model will produce characteristic projected distributions  $P(r)$  resulting, in principle, in different RBS-C responses. We will examine this feature in the framework of the two-beams formulation [20]. For a given axial or planar direction, the spectrum yield (normalized to the amorphous) at the depth  $z$  is given by

$$\chi(z) = \chi_R(z) + [1 - \chi_R(z)]n^*(z), \quad (1)$$

where  $n^*$  is the *effective* relative concentration of scattering centres and  $\chi_R$  is the dechannelled

Table 1

The parameters of the  $\langle 100 \rangle$  and  $\langle 110 \rangle$  projected distributions of the lattice atoms  $P(r)$  computed for a  $20 \times 20 \times 20$  atoms Si supercell with one defect placed in the centre

| Defect          | $\langle 100 \rangle$ |                                      |                 |                                  | $\langle 110 \rangle$ |                                      |                 |                                  |
|-----------------|-----------------------|--------------------------------------|-----------------|----------------------------------|-----------------------|--------------------------------------|-----------------|----------------------------------|
|                 | SD                    |                                      | LD              |                                  | SD                    |                                      | LD              |                                  |
|                 | $n_{\text{SD}}$       | $\langle r^2 \rangle (\text{\AA}^2)$ | $n_{\text{LD}}$ | $\langle r \rangle (\text{\AA})$ | $n_{\text{SD}}$       | $\langle r^2 \rangle (\text{\AA}^2)$ | $n_{\text{LD}}$ | $\langle r \rangle (\text{\AA})$ |
| $I_{\text{H}}$  | 5                     | 0.029                                | 1               | 0.47                             | 3.5                   | 0.037                                | 0.5             | 1.13                             |
| $I_{\text{T}}$  | 4                     | 0.069                                | 0               | –                                | 8                     | 0.038                                | 0.5             | 1.69                             |
| $I_{\text{S}}$  | 6.7                   | 0.030                                | 2               | 0.84                             | 5.7                   | 0.035                                | 1               | 1.36                             |
| $I_{\text{4b}}$ | 40                    | 0.041                                | 8               | 0.86                             | 45                    | 0.051                                | 1               | 0.78                             |
|                 |                       |                                      | 4               | 0.56                             |                       |                                      | 1               | 1.23                             |
| BD              | 2                     | 0.020                                | 2               | 0.88                             | 1                     | 0.029                                | 2               | 0.75                             |
|                 |                       |                                      |                 |                                  |                       |                                      | 1               | 1.09                             |
| Vacancy         | 4                     | 0.022                                | 0               | –                                | 2                     | 0.033                                | 1               | 0.56                             |
|                 |                       |                                      |                 |                                  |                       |                                      | 0               | 0.75                             |
|                 |                       |                                      |                 |                                  |                       |                                      | 1               | 1.13                             |
|                 |                       |                                      |                 |                                  |                       |                                      | 0               | –                                |

$n_{\text{SD}}$  is the number of slightly displaced (SD) atoms ( $\rho < r < R_{\text{L}}$ ) characterized by a mean square displacement  $\langle r^2 \rangle$ .  $n_{\text{LD}}$  is the number of largely displaced (LD) atoms ( $r > R_{\text{L}}$ ) characterized by a mean displacement  $\langle r \rangle$ .

fraction of the beam. Usually, defects are considered as randomly distributed atoms in an unperturbed lattice and  $n^*$  is given as an estimate of the relative concentration of defects. Actually, for a given interstitial model and a small concentration of defects

$$n^* = n_{\text{d}}(f_{\text{SD}} + f_{\text{LD}}), \quad (2)$$

where  $n_{\text{d}}$  is the relative concentration of defects and  $f_{\text{SD}}$  and  $f_{\text{LD}}$  are the average scattering factors of the SD and LD atoms respectively. For axial alignment, the SD atoms contribution is given by

$$f_{\text{SD}} = n_{\text{SD}} \sum_{r=\rho}^{R_{\text{L}}} \frac{P(r)\Phi(r)}{n_{\text{SD}}}, \quad (3)$$

where  $n_{\text{SD}}$  is the number of SD atoms per defect and  $\Phi(r)$  is the channeled ions flux distribution. For small  $r$  [1]:

$$f_{\text{SD}} \propto n_{\text{SD}} \sum_{r=\rho}^{R_{\text{L}}} \frac{P(r)(r/r_0)^2}{n_{\text{SD}}} = n_{\text{SD}} \frac{\langle r^2 \rangle}{r_0^2}, \quad (4)$$

where  $r_0$  is the channel radius. In the case of vacancy-type defects, only the SD atoms contribute to the beam scattering. The LD atoms contribution is given, to a first approximation, by

$$f_{\text{LD}} = n_{\text{LD}} \sum_{r=R_{\text{L}}}^{r_0} \frac{P(r)\Phi(r)}{n_{\text{LD}}}, \quad (5)$$

where  $n_{\text{LD}}$  is the number of LD atoms per defect. For directions with no cylindrical symmetry the 2-D flux and atom distributions must be used in Eq. (5).

The validity of Eq. (2) has been verified by MC-BCA simulation of 2 MeV He  $\langle 100 \rangle$  channeling in supercells populated with constant concentrations of  $I_{\text{S}}$  interstitials (and vacancies) from surface to 400 nm depth. Simulations were also performed on the same supercells by removing either the LD atoms or the SD atoms (and replacing them with ideal lattice atoms). In Fig. 2 the simulated  $n^*$  at the surface obtained by inversion of Eq. (1) are plotted as a function of  $n_{\text{d}}$ . In this case  $\chi_{\text{R}}$  ( $z = 0$ ) is equal to the virgin yield  $\chi_{\text{V}}$ . The separate contributions of LD atoms (dashed line) and SD atoms (dotted line) are also displayed. In the whole concentration range  $n^*$  is exactly the sum of the LD and SD contributions. Moreover, it can be seen that the SD contribution is linear up to about 3%–4%  $I_{\text{S}}$  concentration. For higher concentrations the approximation of a lattice distortion localized around the defect fails. For a given defect model,  $n^*$  will be, in general, dependent on the alignment, therefore the plot of the experimental  $n^*$  values as a function of the alignment can give a signature of the defects present in the sample, even if the most significant LD contribution cannot be separated by the SD one in experimental

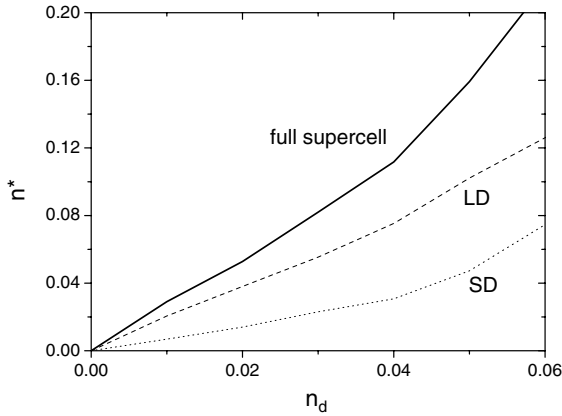


Fig. 2. Effective relative concentration of scattering centres  $n^*$  (heavy line) as a function of the number of interstitials  $n_d$ . The data were extracted from the surface yield of the MC-BCA simulated  $\langle 100 \rangle$  spectra of different supercells populated with a constant concentrations of  $I_S$  defects. The separate contributions of LD atoms (dashed line) and SD atoms (dotted line) are also displayed.

data. Examples of the application of this formulation will be given in the next section.

#### 4. Application to real samples

In order to extract information from a RBS-C spectrum it is necessary to have defect concentrations exceeding 1%. At this level, interaction among defects is already effective and some additional problems, not considered in the previous section, should be considered. The inspection of supercells populated with  $n_d \geq 1\%$  shows that, under defects interaction, the number and the displacement of the SD atoms increase and their distribution becomes isotropic. Moreover, by increasing the concentration, an increasing number of SD lattice atoms undergo large displacements thus entering into the LD population. On the other hand, interstitial atoms slightly move from their original position and, even if they essentially preserve their identity, their projections become less specific. In particular there is an evident evolution of the  $I_T$  defect toward the  $I_H$  configuration, energetically favored for the EDIP potential.

In Fig. 3 the  $\langle 100 \rangle$  aligned RBS-C experimental spectra of the virgin and damaged samples are

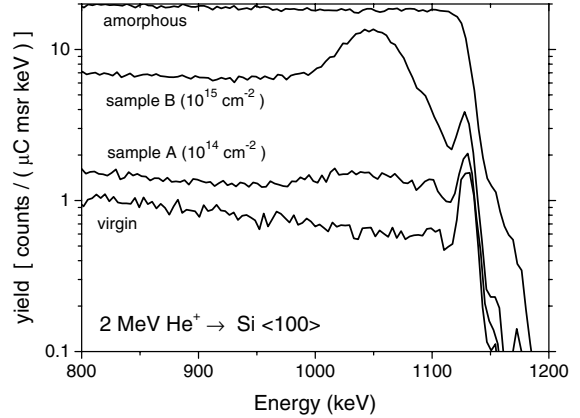


Fig. 3. 2 MeV  $\langle 100 \rangle$  RBS-C experimental spectra for the samples implanted with 180 keV  $\text{Si}^+$  ions at a fluence of  $10^{14} \text{ cm}^{-2}$  (sample A) and  $10^{15} \text{ cm}^{-2}$  (sample B). The spectra of a virgin and an amorphous Si sample are shown for comparison.

displayed together with the spectrum of an amorphous sample. For each defect model, the simulation program required different defect depth profiles to fit the experimental  $\langle 100 \rangle$  spectrum. These defect depth profiles differ in the integral but have the same shape. For each defect model again, spectra were simulated for the other eight alignments by keeping constant the defect depth profile fitted on the  $\langle 100 \rangle$  direction.

##### 4.1. Low damage

For sample A, the  $n^*$  were computed at a depth of 200 nm, corresponding to the peak of the defect depth profile, by inversion of Eq. (1); the procedure employed to estimate the dechanneled fraction of the beam has been described in [19]. The concentration of interstitials ( $n_d$ ) ranged from 1% to 4% depending on the defect model.

In Fig. 4 we show the experimental  $n^*$  values as a function of the alignment. As a reference, we also computed the  $n^*$  for the random model ( $f = 1$ ). We obtained a constant value within 16% standard deviation and we used this figure as an estimation of the uncertainty associated with the experimental points. The plot has a characteristic shape that we can identify as a signature of the defects present in the sample; on the basis of the strong anisotropy of the data we can exclude a significant presence

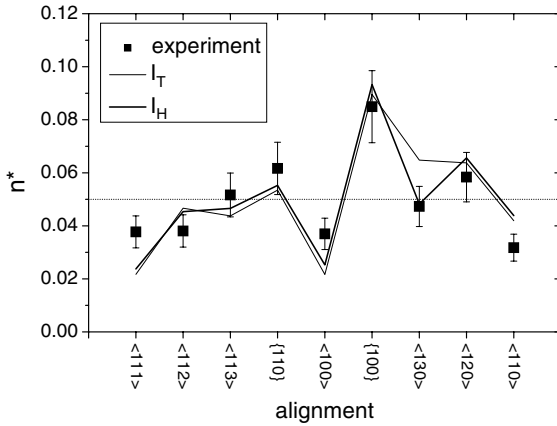


Fig. 4. Effective relative concentration of scattering centres  $n^*$  extracted from the experimental spectra of sample A (squares) and the simulated spectra for the  $I_H$  (heavy line) and  $I_T$  (light line) defects as a function of the alignment. The dotted line represents the isotropic response of the random model.

of amorphous regions in the sample. In Fig. 4 we also show the  $n^*$  values computed from the spectra simulated with the  $I_H$  and the  $I_T$  models. The points are connected with a light and a heavy continuous line respectively to guide the eyes. Our choice of extracting the defect depth profiles from the (100) experimental spectra is arbitrary and, in general, this did not lead to the best fitting over the whole alignments. For this reason, when required, the simulated  $n^*$  datasets were multiplied by a constant value in order to have the same average value of the experimental one (dotted line). This is equivalent to slightly modify the  $n_d$  concentration in Eq. (2). We can observe, as expected from the considerations about the defect interaction, that the supercells populated with  $I_H$  and the  $I_T$  defects almost give the same signature, characteristic of the  $I_H$  site even if an evident difference still persists along the  $\langle 130 \rangle$  axis. This signature is clearly far from the experimental data; in particular there is no evidence of the strong response of the  $\langle 110 \rangle$  alignment with respect to the  $\langle 100 \rangle$  and  $\langle 111 \rangle$  ones, typical of the  $I_T$  and  $I_H$  defects.

In Fig. 5 we show the  $n^*$  values computed from the spectra simulated with the  $I_S$  (light continuous line), the  $I_{4b}$  (heavy continuous line) and the BD (dotted line) models. The first two models are in agreement with the experimental signature,

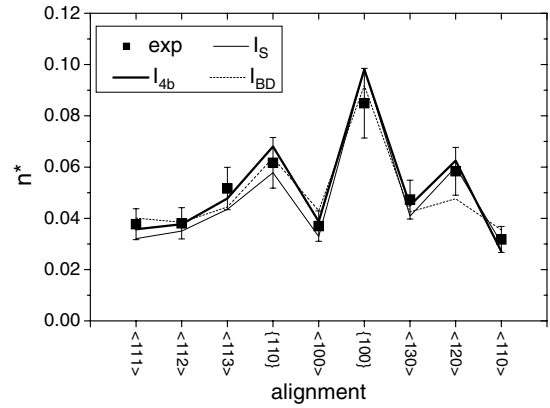


Fig. 5. Effective relative concentration of scattering centres  $n^*$  extracted from the experimental spectra of sample A (squares) and the simulated spectra for the  $I_{4b}$  (heavy line),  $I_S$  (light line) and BD (dashed line) defects as a function of the alignment.

whereas the BD dataset has two points outside the error bars even if the general trend is similar.

The above results indicate that, at least in the case of practical low concentrations of defects, self-interstitial atoms in silicon (as modeled by the EDIP potential) are spatially located in the neighborhood of two sites, we may label as the  $I_H$ -site and the  $I_S$ -site. In sample A we unambiguously detected the presence of  $I_S$ -site defects. It is worth noting that also in the case of the  $I_{4b}$  defect, which derives from the aggregation of split- $\langle 100 \rangle$  interstitials, the position of the LD atoms are close to the  $I_S$ -site.

As the LD atoms give the main contribution to the spectrum yield, we can conclude that the RBS-C technique can clearly identify three groups of defects (amorphous regions,  $I_H$ - and the  $I_S$ -site interstitials). The possibility to discriminate among the different defect models within a given group needs instead further investigation. For a higher selectivity one could compare the yield of the experimental (4% uncertainty) and simulated spectra. In this case none of the simulations based on the defect models here considered could fit all the nine experimental spectra within the errors even if both  $I_S$  the  $I_{4b}$  were in reasonable agreement. At this level the RBS-C seems to be very sensitive but the complexity of the problem and the uncertainty connected to the present defect modeling does not allow for

exploiting the full potentialities of the technique. As the atomic location can only give a partial answer to the problem of defect recognition, the simultaneous use of different techniques, sensitive to either the number of interstitials or the different properties of the defects, should be envisaged.

#### 4.2. High damage

The extension of the procedures used so far to the case of highly defective samples needs special care and it is discussed in detail in [21]. A supercell populated with a high concentration of defects and relaxed by static minimization (equivalent to 0 K molecular dynamics) may preserve too much memory of the initial configuration. In the case of the  $I_S$  defect, for example, the energy of the simulated sample already exceeds the energy of the amorphous phase for concentrations larger than 10%, indicating that we are dealing with a highly metastable system. Keeping in mind these limitations, it is however possible to qualitatively analyze sample B. For 200 nm depth, we compare the responses of simulations based on both the  $I_S$  model ( $n_d \cong 17\%$ ) as representative of the  $I_S$  family detected at low fluence and the random model ( $n_d \cong 70\%$ ) with the experimental ones. It is still possible to apply the same formulation used for sample A, provided that a proper dechanneling function is used [22]. The differences between the random and the  $I_S$  model, as shown in Fig. 6, are small but still evident in the directions lying on the  $\{100\}$  plane. Moreover, we can observe that the experimental points are located between the two simulations suggesting that simple defects and amorphous regions could coexist. This hypothesis is in agreement with the findings of [23,24] on a similar set of implantation conditions.

## 5. Conclusions

We have reviewed a recent development of the standard MC-BCA method, concerning the insertion of realistic defective structures in the simulation of RBS-C spectra. In the case of low-fluence self-ion implantation of silicon we have demonstrated that multi-axial measurements can unambiguously discriminate among three classes of small defects, characterized by their spatial locations. In particular, in the present experiment we detected the presence of  $I_S$ -site interstitials. In the case of highly defective samples, even if the structural description of the system needs further investigation, we could argue the coexistence of simple defects and amorphous regions. The encouraging results suggest that other studies, such as the defect-impurity interaction [25] and the annealing of defects, could also benefit the synergy between atomic-scale modeling and the ion channeling techniques.

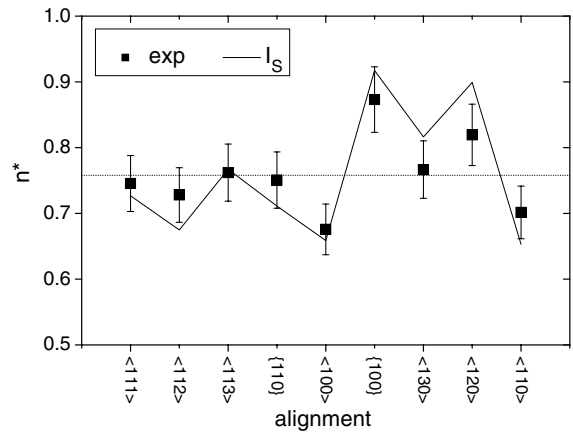


Fig. 6. Effective relative concentration of scattering centres  $n^*$  extracted from the experimental spectra of sample B (squares) and the simulated spectra for  $I_S$  defects (light line) as a function of the alignment. The dotted line represents the isotropic response of the random model.

biguously discriminate among three classes of small defects, characterized by their spatial locations. In particular, in the present experiment we detected the presence of  $I_S$ -site interstitials. In the case of highly defective samples, even if the structural description of the system needs further investigation, we could argue the coexistence of simple defects and amorphous regions. The encouraging results suggest that other studies, such as the defect-impurity interaction [25] and the annealing of defects, could also benefit the synergy between atomic-scale modeling and the ion channeling techniques.

## Acknowledgements

The authors wish to thank R. Lotti and S. Cristiani for the samples implantation. This work was partially supported by MIUR under the FIRB (RBAU01LLX2) project.

## References

- [1] L.C. Feldmann, J.W. Mayer, S.T. Picraux (Eds.), Material Analysis by Ion Channeling, Academic Press, New York, 1982.
- [2] J.R. Tesmer, M. Nastasi (Eds.), Handbook of Modern Ion Beam Materials Analysis, Materials Research Society, Pittsburgh, PA, 1995.

- [3] J.H. Barret, *Phys. Rev. B* 3 (1971) 1527.
- [4] P.J.M. Smulders, D.O. Boerma, *Nucl. Instr. and Meth. B* 29 (1987) 471.
- [5] E. Albertazzi, M. Bianconi, G. Lulli, R. Nipoti, M. Cantiano, *Nucl. Instr. and Meth. B* 118 (1996) 128.
- [6] L. Colombo, *Ann. Rev. Mater. Res.* 32 (2002) 271.
- [7] S.K. Estreicher, *Mater. Today* 6 (2003) 26.
- [8] R.S. Averback, T. Diaz de La Rubia, *Solid State Phys.* 51 (1998) 281.
- [9] B. Weber, E. Wendler, K. Gärtner, D.M. Stock, W. Wesch, *Nucl. Instr. and Meth. B* 118 (1996) 113.
- [10] R. Jones, T.A.G. Eberlein, N. Pinho, B.J. Coomer, J.P. Goss, P.R. Briddon, S. Öberg, *Nucl. Instr. and Meth. B* 186 (2002) 10.
- [11] S. Balboni, E. Albertazzi, M. Bianconi, G. Lulli, *Phys. Rev. B* 66 (2002) 045202.
- [12] G. Lulli, E. Albertazzi, M. Bianconi, G.G. Bentini, R. Nipoti, R. Lotti, *Nucl. Instr. and Meth. B* 170 (2000) 1.
- [13] J.F. Justo, M.Z. Bazant, E. Kaxiras, V.V. Bulatov, S. Yip, *Phys. Rev. B* 58 (1998) 2539.
- [14] N. Arai, S. Takeda, M. Kohyama, *Phys. Rev. Lett.* 78 (1997) 4265.
- [15] A. Bongiorno, L. Colombo, F. Cargnoni, C. Gatti, M. Rosati, *Europhys. Lett.* 50 (2000) 608.
- [16] M. Tang, L. Colombo, J. Zhu, T. Diaz de la Rubia, *Phys. Rev. B* 55 (1997) 14279.
- [17] D.M. Stock, B. Weber, K. Gärtner, *Phys. Rev. B* 61 (2000) 8150.
- [18] L.A. Marqués, L. Pelaz, J. Hernández, J. Barbolla, G.H. Gilmer, *Phys. Rev. B* 64 (2001) 045214.
- [19] G. Lulli, E. Albertazzi, M. Bianconi, A. Satta, S. Balboni, L. Colombo, *Phys. Rev. B* 69 (2004) 165216.
- [20] E. Bøgh, *Can. J. Phys.* 46 (1968) 653.
- [21] G. Lulli, E. Albertazzi, M. Bianconi, A. Satta, S. Balboni, L. Colombo, A. Uguzzoni, these Proceedings, doi:10.1016/j.nimb.2004.12.110.
- [22] M. Bianconi, R. Nipoti, M. Cantiano, A. Gasparotto, A. Sambo, *Nucl. Instr. and Meth. B* 84 (1994) 507.
- [23] O.W. Holland, S.J. Pennycook, G.L. Albert, *Appl. Phys. Lett.* 55 (1989) 2503.
- [24] L. Sealy, L.C. Barklie, G. Lulli, R. Nipoti, S. Milita, M. Servidori, *Nucl. Instr. and Meth. B* 96 (1995) 215.
- [25] A. Satta, E. Albertazzi, M. Bianconi, G. Lulli, S. Balboni, L. Colombo, these Proceedings, doi:10.1016/j.nimb.2004.12.027.